PbS nanocubes for solar energy storage

Amira Lemsi,[1] Drialys Cárdenas-Morcoso,[2] Marta Haro,[3] Carlos Gil-Barrachina,[2] Clara Aranda,[2] Hager Maghraoui-Meherzi,[1] Miguel García-Tecedor,[2,*] Sixto Giménez,[2,*] Beatriz Julián-López[2,*]

[1] Université de Tunis El-Manar, Faculté des Sciences de Tunis, Laboratoire de Chimie Analytique et d'électrochimie LR99ES15, Campus Universitaire de Tunis El-Manar,2092 Tunis, Tunisia

[2] Institute of Advanced Materials (INAM), Universitat Jaume I, 12006 Castelló, Spain

[3] Instituto de Ciencia de Materiales de Aragón (ICMA) Universidad de Zaragoza, Zaragoza 50009, Spain

[*]Corresponding author: tecedor@uji.es, sjulia@uji.es, julian@uji.es

Abstract

PbS nanocubes have been produced by a very simple solvothermal procedure that employs a unique molecule, ethylenediamine, as solvent and capping ligand to control the size and shape of nanocrystals. Detailed structural, optical and photoelectrochemical evaluation confirmed the suitability of these nanoparticles for photocapacitive applications, when synergistically combined with spin-coated $BiVO_4$ photoelectrodes, as derived from the estimated energy diagram. Furthermore, the p-n junction facilitates the photo-oxidation of PbS nanoparticles under light irradiation. In the dark, the photogenerated charges are released providing an electric output response with a solar-to-current efficiency of 0.042 %, storing energy extra to the H_2 produced by water splitting when the $BiVO_4$ photoanode works under illumination. This study highlights the importance of the synthetic route and methodology to ensemble materials for advanced solar energy storage applications.

This article has been accepted for publication and undergone full peer review but has not been through the copyediting, typesetting, pagination and proofreading process, which may lead to differences between this version and the Version of Record. Please cite this article as doi: 10.1002/ente.202000301

Introduction

The current energy scenario based on fossil fuels is practically exhausted, leading to undesirable consequences as the decrease of the oxygen level in the oceans, melting the ice in the poles and leaving a quarter of the world´s population at risk of water supply problems or floods, as it was recently addressed in the 2019 United Nations Climate Change Conference, COP25. In this context, the development of safe and sustainable energy storage constitutes one of the most relevant technological challenges of the XXI century. Provided that fossil fuels cannot provide sustainable source of clean energy to meet our future demands, the proper matching of energy demand and energy supply requires that inherently intermittent renewable resources like solar light or wind must be efficiently stored into batteries (electrical storage) or fuels (chemical storage). Consequently, the development of global strategies to provide sustainable solutions for renewable energy storage has gained lot of interest in the last years, with impressive advances in the field of solar fuels,[1] electrosynthesis of added value products,[2] and electrochemical valorization of waste.[3] Identically, electrical storage has significantly progressed in particular meeting the needs for wearable,[4] transport,[5] and residential applications.[6] Critical issues like long-term cyclability[7] and cost[8] have been recently reviewed in order to provide a technologically and economically robust solution for different applications. On the other hand, storage of solar energy in electrochemical devices like redox-flow batteries is also at the forefront of the research in novel energy storage systems, with tailored redox reactions, which overcome some of the thermodynamic and kinetic limitations intrinsic to more complex electrochemical reactions, like water spitting.[9] Recently, the possibility to increase the efficiency of Z-scheme water splitting photoelectrochemical cell by combination with a flow battery was proposed, showing that it is possible to store the photocharges "loss" in OER and HER side-reactions as chemical energy.[9b]

In this context, lead based materials (halides, chalcogenides, oxides, etc…) stands out as promising materials, which have demonstrated excellent optoelectronic properties for different energy conversion and storage applications. The most remarkable example of lead based materials for energy conversion applications relates to lead halide perovskites, which have experienced in the last years a remarkable increase of photovoltaic efficiencies up to 25.2 %,[10] and light emission with external quantum efficiency over 20%,[11], and its charge storage properties have also been highlighted.[12]

Another exciting Pb based material for energy conversion is lead sulfide (PbS). Lead sulfide is a binary IV-VI semiconductor material, with small direct bandgap (0.41 eV) and large exciton Bohr radius of 18 nm, compared to many semiconductors. This material has been successfully used for different applications such as infrared sensors,[13] solar cells,[14] light emitting diodes,[15] nanoscale lasers,[16] photonic and optical switches,[17] and biological imaging[18] due to its controllable size and morphology. Indeed, lead sulfide has been produced with different morphologies at nanometer- to micrometer scale such as: rods,[19]needles,[20] wires,[21] octahedrons,[22] dendritic stars[22-23] and cubes,[23b] by several synthetic methods (e.g.: microwave, hydrothermal, solvothermal and chemical or thermal decomposition routes,[19b, 24]) under different reaction conditions (lead and sulphur precursors, temperature, time, solvent, surfactants, capping ligands...).

For practical applications in electrochemical devices, it is important to prepare stable colloidal PbS dispersions in order to get densely packed nanocrystal thin films with isotropic properties. Thus, PbS nanocubes appear to be an interesting shape for efficient spatial arrangement,[25] although other interesting morphologies have been reported.[26] Scarce information on the fabrication of PbS nanocubes is found in the literature. In 2006, the preparation of PbS nanocubes by a surfactant AOT-assisted solvothermal route was reported.[27] Later, PbS nanocubes were generated in oleylamine and dodecanethiol from decomposition of a very complex lead precursor, $Pb(pic)_2tu$.[23b] Both studies employ the solvothermal methodology, which is a very promising due to its low cost, high efficiency and its potential for large-scale production. However, very exotic and complex precursors and surfactants needed to be employed.

This manuscript reports on the synthesis of highly uniform PbS nanocubes by a very simple solvothermal procedure that employs a unique molecule, ethylenediamine, as solvent and capping ligand to control the size and shape of nanocrystals. The tuning of reaction parameters (i.e. temperature and time of solvothermal digestion) and the ratio of reagents affords homogeneous nanocubes. The cubic structure facilitates the assembly of PbS nanoparticles on $BiVO_4$ photoanode, extensively used in solar water splitting. PbS/$BiVO_4$ forms a p-n junction that promotes the oxidation of PbS in place of OER. Oxidized PbS nanoparticles are reduced in the dark providing an output energy of 0.35 $\mu Wh/cm^2$. The photocapacitive response of PbS-$BiVO_4$ photoanodes was

previously reported by us,[28] showing herein a simpler, cheaper and more controlled synthesis of energy harvested photoanodes for water splitting.

Experimental method

Synthesis of PbS nanoparticles:

Lead (II) acetate trihydrate ($Pb(CH_3COO)_2 \cdot 3H_2O$), thioacetamide ($C_2H_5NS$, TAA), ethylenediamine (EDA) were purchased from Sigma-Aldrich and used as received. In a typical synthesis, 0.3783g of $Pb(CH_3COO)_2 \cdot 3H_2O$ and 0.0751 g of C_2H_5NS were independently dissolved in 15mL of EDA respectively, and then mixed together. The initial transparent solution turns into dark color immediately after mixing. After 30 minutes of stirring, the mixture was transferred into a 45 mL Teflon-lined stainless-steel autoclave, sealed and heated at 180ºC for 16 hours. A black precipitate was collected by centrifugation. The product was repeatedly washed with ethanol and water, and dried at 80°C overnight. These synthetic parameters were previously optimized in order to achieve a good control on the morphological properties of the nanocubes. The details of these preliminary studies performed on the synthesis are found in the supporting information file.

Synthesis of $BiVO_4$ and $BiVO_4$/PbS thin films:

Thin films of $BiVO_4$ and $BiVO_4$/PbS were deposited onto fluorine-doped tin oxide (FTO) substrates through spin coating method. The $BiVO_4$ precursor solution was prepared as previously reported.[29] First, commercial bismuth (III) nitrate pentahydrate, $Bi(NO_3)_3 \cdot 5H_2O$, (Sigma Aldrich, reagent grade, 98%) was used to prepared a transparent 0.2 M solution in glacial acetic acid, after 10 min of ultra-sonication. Secondly, a commercial vanadyl acetylacetonate, $VO(acac)_2$, (Sigma-Aldrich 98%) was used to prepare a dark green 0.2 M solution in acetyl acetone, after 20 min of ultra-sonication. Both solutions were mixed and sonicated during 20 min until complete homogeneity and finally filtered through a polytetrafluoroethylene (PTFE) membrane of 0.22 µm pore size.

For the $BiVO_4$ film deposition, FTO substrates were cleaned by ultra-sonication in Hellmanex detergent, Milli-Q water and in a solution of ethanol:isopropanol (1:1 v/v). Prior to the deposition of the active layer, substrates were treated in a UV–O_3 cleaner for 15 min. 100 µl of the $BiVO_4$ precursor solution was deposited by spin-coating at 1000 rpm-800rpm/s during 15s followed by annealing at 450 °C/30 min in a hot plate.

This process was repeated to complete 10 cycles, being the last one annealed at 450ºC during 5 hours in a box furnace to ensure the monoclinic-scheelite structure.

PbS thin films were deposited using a 20 mg/ml solution of PbS in ethanol, which provided the best dispersability among different tested solvents (**Supporting Information, Figure S1a)**. 20 μL of the solution were deposited onto the $BiVO_4$ films and also directly onto FTO substrates by spin coating at 6000 rpm during 15s followed by an annealing step at 80ºC during 10 min, in order to remove the excess of the solvent.

Structural, optical and electrochemical characterization.

XRD diffraction data was carried out with a D4 Endeavor system (Bruker-AXS) with Cuk_α radiation (λ= 1.5406 Å). The morphology of the different samples was analyzed with a JEOL JEM-3100 Field Emission Scanning Electron Microscope (FEG-SEM) including EDS analysis. Transmission Electron Microscopy (TEM) was performed with a JEOL 2100 instrument, operating at 100 kV.

Dynamic light scattering (DLS) experiments were performed on a Zetasizer Nano ZS from Malvern Instruments (λ= 633 nm). For the a nalysis, PbS nanocrystals were dispersed in ethanol at a concentration of 50 ppm and poured into a standard plastic cuvette. The temperature was fixed at 20ºC and the measurement was repeated three times for each sample.

Fourier-transform Infrared (FTIR) spectra was collected on a FT/IR-6200 from Jasco. For the analysis, several drops of the PbS ethanolic suspensions were deposited on a KBr pellet and evaporated by an IR lamp. The spectra were recorded by transmittance from 4000 to 400 cm^{-1}, with a resolution of 1cm^{-1} and accumulation of 64 scans.

The optical properties of the prepared PbS colloidal solutions and films were also determined using a Lambda 1050+ Perkin Elmer UV/Vis/IR spectrophotometer. The absorbance (A) of the thin films was estimated from transmittance (T) and diffuse reflectance (R) measurements using an integrating sphere as $A = -\log(T + R)$. The direct optical band gap was estimated by the Tauc plot as $(h\nu)^{1/n} = A(h\nu - E_g)$, where n = 1/2 for direct transitions.

Electrochemical and photoelectrochemical measurements were performed using an Autolab potentiostat/galvanostat PGSTAT302 workstation, coupled to a 300 W Xe

lamp for experiments under illumination conditions, adjusting the light intensity to 100 mW cm^{-2} using a thermopile. Unless otherwise specified, the measurements were carried out in a three-electrode cell, where the sample under test, an Ag/AgCl (KCl 3M) electrode and a Platinum wire were used as working, reference and counter electrode, respectively. All the potentials have been referred to the Reversible Hydrogen Electrode (RHE) electrode using the Nernst equation: $V_{RHE} = V_{Ag/AgCl} + V^0_{Ag/AgCl} + 0.059 \cdot pH$. The electrolyte employed was 0.1M Na_2S and 0.1M Na_2SO_3 at pH= 13.4 for the characterization of the PbS films, while a potassium phosphate buffer (K-Pi) at pH 7 was used to characterize the PbS-PbO_x/$BiVO_4$ system. These testing conditions were key to prevent the detachment of the PbS/PbO_x nanocubes from $BiVO_4$ during electrochemical testing. Cyclic voltammetry measurements were performed at a scan rate of 50 mV s^{-1} and 5 mV step. Electrochemical impedance spectroscopy (EIS) was performed between 0.01 Hz and 40 kHz with 20 mV amplitude perturbation. Mott-Schottky analysis was carried out using the expression (for an n-type semiconductor):

$$\frac{1}{C_{SC}^2} = \frac{2}{\varepsilon_0 \varepsilon_r e N_D A^2}\left(\phi_{SC} - \frac{kT}{e}\right)$$

where C_{SC} represents the space charge capacitance, ϕ_{SC}=V-V_{FB} is the voltage drop at the space charge region, V is the applied potential, V_{FB} the flat band potential, N_D the donor density, e the elementary charge, ε_0 the permittivity in vacuum, ε_r is the relative permittivity of the material, taken as 190 for PbS,[30] and 68 for $BiVO_4$,[31] A is the electrode area, k is the Boltzmann constant and T is the absolute temperature, taken as 298 K.

Results and discussion

PbS nanocrystals were prepared from precipitation of lead acetate and thioacetamide as sources of Pb^{2+} and S^{2-} ions, respectively, in an organic aminated medium (ethylenediamine), without further purification. The crystal formation occurred immediately after mixing both reagents at room temperature (25ºC), but highly anisotropic platelets were initially generated (see **Supporting Information, Figure S2**a), suggesting a kinetic growth regime with a fast unidirectional growth. This effect was previously reported for PbS obtained through decomposition of lead xanthates in long-chained amines.[32] Then, a solvothermal treatment at higher temperature (110ºC, 180º C or 300ºC; SEM images showed in **Supporting Information, Figure S2**b-d) was

carried out in order to partially redissolve these anisotropic structures and precipitate PbS under more controlled conditions. This process of redisolution-nucleation is known as Ostwald ripening mechanism,[33] which occurs upon thermodynamic equilibrium conditions. At this point, the use of ethylenediamine (EDA) as solvent and bidentate capping ligand played a key role on the morphological properties of the PbS particles. This molecule was already employed for the preparation of CdS[34] and PbS[35] nanostructures. EDA is a highly nucleophilic agent that attacks Pb from the acetate precursor affording the $[Pb(EDA)_2]^{2+}$ complex. After thioacetamide addition, the EDA ligand is replaced by this ligand because of its higher affinity for Pb^{2+} compared to amino-based ligands, according to Pearson's HSAB theory. These sulphur-based Pb^{2+} complexes rapidly evolve towards the formation of PbS crystals. These intermediate Sulphur-based Pb^{2+} species were detected as yellow complexes when reaction takes place at low temperature (0 ºC), as shown in **Supporting Information, Figure S3**. PbS crystallizes as a rock-salt cubic structure, but upon heating and the interaction of ethylenediamine at the surface of the seeds, the growth on the (111) faces is favored, and the cubic shape is facilitated. [22, 36] After several washing steps, FTIR analysis of the dried nanocubes was performed (**Supporting Information, Figure S4**). No clear signal of EDA or TAA molecules grafted at the surface of the nanocubes was observed, but we cannot completely exclude the presence of some inorganic or short chain organic ligands from the reaction medium that help their further dispersion in ethanol.

To further understand the role of EDA in our synthesis, several organic amines with different lengths and number of amine-coordinating groups located at different positions (DAP: 1,3-diaminopropane, DETA: diethylenetriamine, TETA: triethylenetetramine, OAM: oleylamine, OA: oleic acid) were tested. Irrespectively of the amine-coordinating group employed, the cubic morphology was observed, as shown in **Supporting Information, Figure S5**. However, the shorter and more rigid EDA molecule provided the best result in terms of small size and uniformity (**Supporting Information, Figure S5**). Finally, the Pb:S ratio was also varied according to previous studies indicating that this ratio modulated the dimensions of rods and dendritic structures.[23b, 37] In our synthesis, the nanocrystals exhibited similar sizes but appeared more rounded with the increasing content of the Sulphur precursor. Consequently, the most uniform cubic shape and smallest particle size were obtained for the stoichiometric Pb:S ratio (1:1) (**Supporting Information, Figure S6**).

Once the synthetic parameters were optimized (180ºC/16h/EDA/1Pb:1S), a complete characterization of structure and capacitive properties was performed. Scanning electron microscopy revealed that well-defined nanocubes with sizes of 40 - 70 nm-edge were obtained, as shown in **Figure 1**. These results are in good agreement with DLS measurements showed as **Supporting Information, Figure S1b**. The powder XRD pattern of the nanocubes (**Figure 1**, inset) confirmed the crystallization of PbS in the face-centered cubic rock-salt structure (ICSD 38293) as single phase. Moreover, very similar XRD patterns were obtained regardless the reaction conditions (see **Supporting Information, Figure S7**). The absence of secondary phases, such as PbO, PbO_2, $PbSO_3$, $PbSO_4$ or residual reagents, confers significant advantages to the present synthetic route, since conversely to other reported methods, where N_2, Ar or vacuum conditions are needed,[17, 38] atmosphere control is not required here. TEM images confirmed the description from SEM evaluation (**Figure 1**). The crystals have cubic shapes of less than 80 nm and each nanocube is a single crystal free of ligands at the surface.

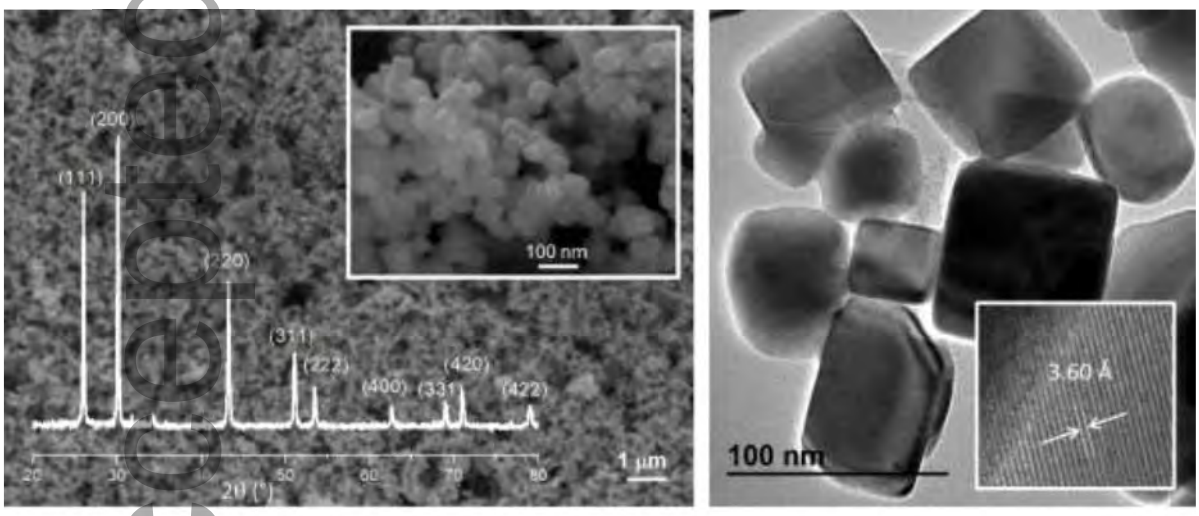

Figure 1.- Structural and morphological characterization of PbS nanocubes: (Left) Powder XRD pattern and SEM image (inset: high magnification); (Right) HR-TEM image (inset: magnification of one PbS crystal showing (111) interplanar distance)

Electrochemical characterization of the PbS films

In order to determine the electrochemical and semiconducting properties of the as-synthesized PbS nanocubes, electrochemical characterization of PbS films on FTO substrates was carried out by cyclic voltammetry and electrochemical impedance. The

cyclic voltammograms of the PbS films (**Figure 2a**,) clearly showed the reduction peak of Pb^{2+} to Pb^0 at – 0.2 V vs RHE (labeled as C_1) according to the reaction:[39]

$$PbS + 2e^- + H_2O \rightarrow Pb^0 + HS^- + OH^- \quad (1)$$

Similarly, the oxidation peak at 0 V vs RHE, (labeled as A_1) corresponds to the oxidation of metallic Pb to Pb^{2+}as:

$$Pb + 2OH^- \rightarrow PbO + H_2O + 2e^- \quad (2)$$

Furthermore, relevant information about the electronic properties of PbS was extracted from Mott-Schottky analysis (**Figure 2b)**. The negative slope of the linear fit indicated the p-type characteristics of PbS in good agreement with previous literature,[40] and the donor density was estimated as N_A=3.8x10^{19} cm^{-3} from the equation $N_A = \frac{2}{\varepsilon_0 \varepsilon_r e m A^2}$, where m the slope of the Mott-Schottky plot. The flat band potential was around 0.55 V vs RHE, also in good agreement with previous reports.[41] Since the flat band potential is related to the Fermi level of majority carriers (holes in a p-type semiconductor), the position of the valence band (E_{vb}) was estimated around 200 mV below the Fermi level, i.e. E_{vb} =0.75 V vs RHE. The optical bandgap of the synthesized PbS nanocubes was calculated from the Tauc plot for direct transitions extracted from the absorption spectrum (**Supporting Information, Figure S8**) as E_g = 0.46 eV, nicely matching the results obtained in previous studies,[42] and consequently, the conduction band (E_{cb}) was located at E_{cb}= 0.3-0.35 V vs RHE. These estimated energy levels have been included in the **Scheme 1**.

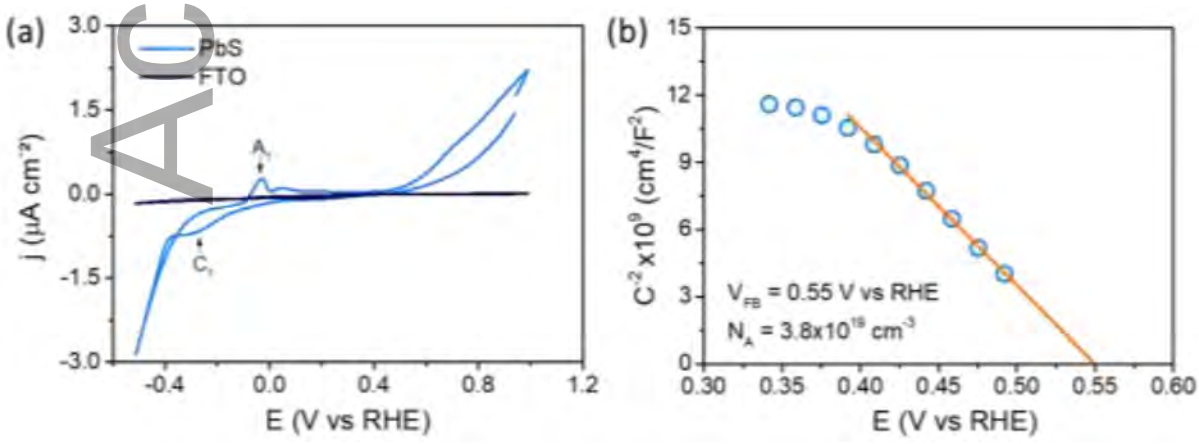

Figure 2.- (a) Cyclic voltammogram (CV) of PbS thin film in a 0.1 M Na_2S and 0.1 M Na_2SO_3 electrolyte at pH 13.4. The CV of the FTO bare substrate is also showed for comparison. (b) Mott-Schottcky plot of the FTO/PbS film, and linear fitting used to extract the donor density (N_D) from the slope and the flatband potential (E_{vb}) from the x-intercept.

Once the basic electrochemical and semiconducting properties of the PbS nanocubes were determined, our aim was employing these PbS nanocubes for solar energy storage. In a previous study, we showed that heterostructuring PbS nanocrystals with $BiVO_4$ films synthesized by electrodeposition, interesting synergistic photocapacitive properties developed in the combined system.[28] In the present study we substituted the PbS quantum dots produced by a much more complex synthetic route by the easily-synthesised PbS nanocubes described above. Furthermore, denser $BiVO_4$ films produced by spin-coating were used in the present study, instead of the more porous electrodeposited $BiVO_4$, employed before.

The structural and optical characterization of the as-prepared $BiVO_4$ films used herein were included in the **Supporting Information, Figures S9-S13**. The spin-coated $BiVO_4$ films on FTO substrates exhibited high coverage and homogeneity (**Figure S9**). Furthermore, the XRD pattern of the spin-coated $BiVO_4$ corresponded to the monoclinic scheelite structure (**Supporting Information, Figure S10**).[29] No trace of other materials, apart from the FTO substrate, or ternary compounds were observed. The optical properties of the deposited $BiVO_4$ films (**Figure S11**a) reflects the increased absorption around 500 nm corresponding to an optical bandgap of 2.5 eV (**Supporting Information, Figure S11b**), in good agreement with other reported values for this material.[43] The Mott-Schottky analysis of the $BiVO_4$ spin-coated films (**Figure S12**) confirmed its n-type characteristics and the values of the donor density ($N_D = 5.43x10^{19}$ cm^{-3}) and flat band potential (V_{FB} = 0.4 V vs RHE) were extracted. These values are also in good agreement with previous studies of $BiVO_4$.[44] From the determination of the optical bandgap from optical measurements and the flatband potential from Mott-Schottky analysis, the energy levels of the spin coated $BiVO_4$ films were determined, and the band alignment on the PbS/$BiVO_4$ architecture is showed in the **Scheme 1**. From this band structure, and considering the p-n junction formed between PbS and $BiVO_4$ interfaces, the photogenerated holes at $BiVO_4$ under illumination should be injected into PbS to form PbO_x.

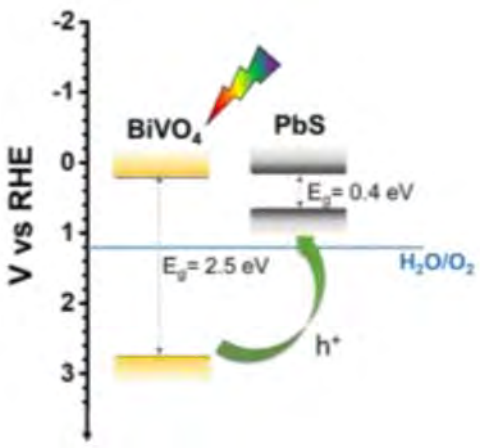

Scheme 1. Schematic representation of the band alignment of the BVO_4/PbS heterostructure.

The morphology of both $BiVO_4$ and $BiVO_4$/PbS was investigated by SEM. $BiVO_4$ thin films were characterized by a granular surface with small grain size of a few hundred nm (**Supporting Information, Figure S13)** and the average thickness of the deposited $BiVO_4$ films was 80 nm (**Supporting Information, Figure S14)**. Upon spin-coating of PbS nanocubes, the surface of the $BiVO_4$ films appeared totally covered by PbS nanoparticles (**Supporting Information, Figure S15a**). Upon electrochemical treatment of the BiVO4/PbS films consisting of 100 cyclic voltammetry scans between -0.6 V vs RHE and 1.8 V vs RHE under illumination in a phosphate buffer electrolyte at pH7, the morphology of the original PbS nanocubes was totally modified (**Supporting Information, Figure S16a**) due to the electrochemical conversion of lead sulfide into lead oxide (PbO_x). At higher magnification, (**Supporting Information, Figures S15b** and **S16b)**, the morphological changes from the initial cubic PbS nanostructures into the PbO_x agglomerates become more evident. These results were consistent with the decrease of the Sulphur content, before and after 100 cyclic voltammetry cycles, measured by EDS (**Supporting Information, Table S1**). EDS shows a final Pb:S:O composition ratio of 0.26:0.22:0.49, which can be attributed to two different or combined phenomena: i) a mixture of $xPbO{\cdot}PbSO_4$ formed during PbS photo-oxidation, since the PbO species can catalyze the photo-oxidation of PbS to $PbSO_4$ forming a mixture of both species,[45] and/or ii) incomplete PbS photo-oxidation caused by the increase of the oxide species modifying the redox potential of the reaction according to Nernst equation, subsequently leading to a competition between OER and PbS oxidation at certain concentration.[46]

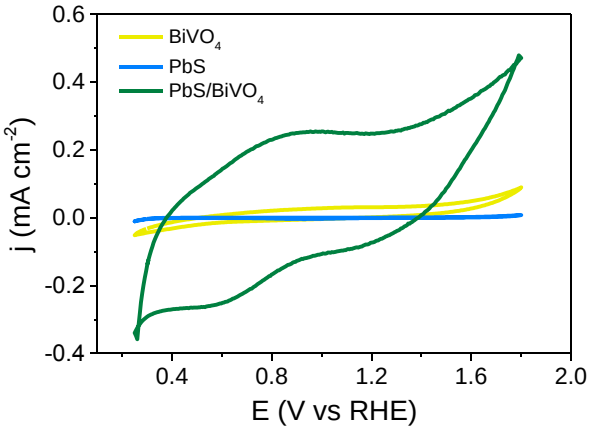

Figure 3. Cyclic voltammogram after 100 cycles, recorded at 50 mV s^{-1} scan rate under illumination, for PbO_x/BiVO4 and the indiviual components PbS and $BiVO_4$ showing the synergistic photocapacitive efect between $BiVO_4$ and PbS. All measurements were performed in K-Pi buffer at pH 7.

After 100 voltammetry scans under illumination, the PbS/$BiVO_4$ CV is not anymore evolving, indicating reversible changes in the photoanode between two oxide states of PbO_x. The evolution of the CV during these 100 scans is shown in **Supporting Information, Figure S17.** The capacitive shape of PbS/$BiVO_4$ CV in **Figure 3** stems from the synergistic interaction between both PbS and $BiVO_4$, since this response was not identified at any of the individual materials tested. Indeed, two bumps are observed in the CV around 0.8 and 0.6 V in the anodic and cathodic current, which can be assigned to the two different oxide states of Pb (2^+ and 4^+) identified in Pourbaix diagrams.[47] These results evidence that photogenerated holes at $BiVO_4$ oxidize the PbO_x into PbO_2, positively charging the surface of the heterostructure (photocharging of the capacitor). In dark conditions, PbO_2 can be reduced to the initial PbO_x by the discharge of the capacitor in a fully reversible process.

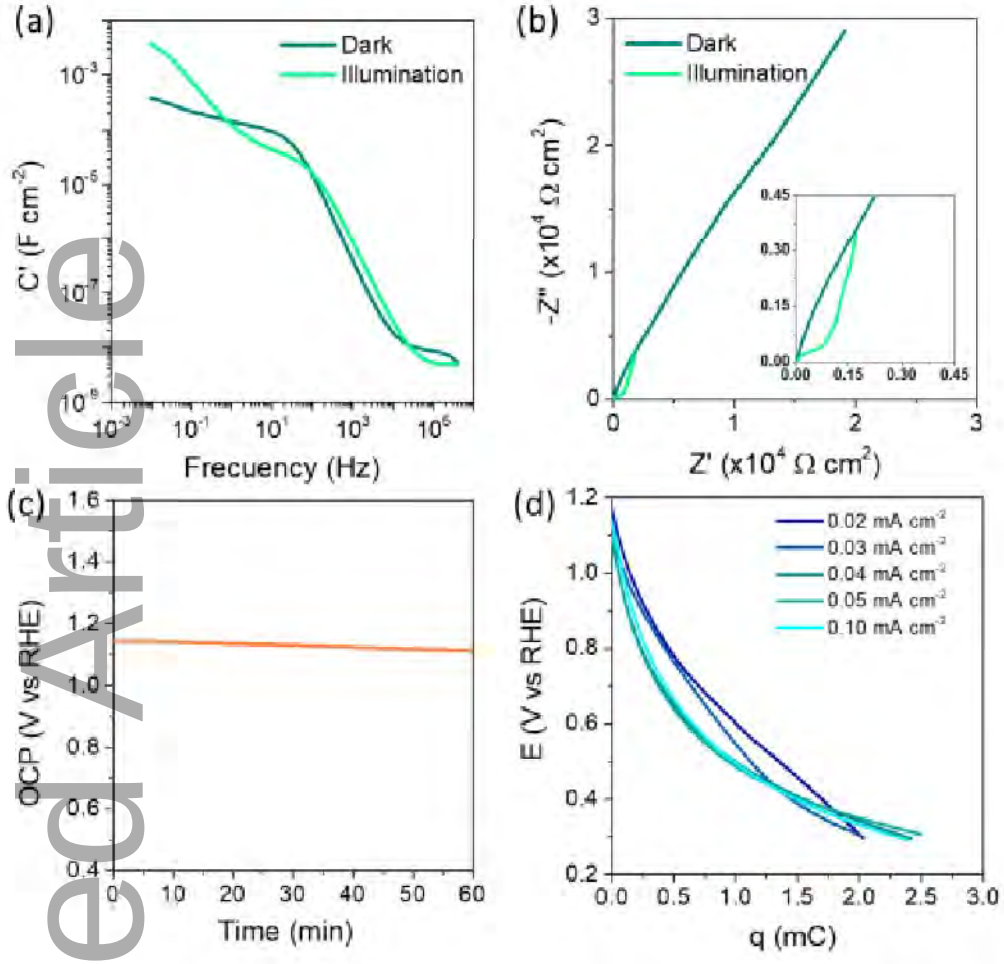

Figure 4.- (a) Bode plot of the real part of the capacitance and (b) Nyquist plot, in the dark and under illumination of the $PbO_x/BiVO_4$ heterostructure at 0.7 V vs RHE; (c) Stability of the OCP measured in dark condition after full photocharging of the $PbO_x/BiVO_4$ electrode; (d) Delivered charge during discharge procedure at different current densities after full charging of the photocapacitor.

The photocapacitance at the $PbO_x/BiVO_4$ photoanode is 4.2 mF cm^{-2} estimated from the CV plot. This value perfectly agrees with that extracted from impedance spectroscopy at the low frequency region (~10 mHz), C = 4 mF·cm^{-2}, see the Bode plot of impedance in **Figure 4a**, performed at 0.7 V vs RHE. This low frequency capacitance is only observed when the system is illuminated and it is associated to the photocharging of the capacitor under illumination. The other plateau at 1-100 Hz and a value around 10^{-4} F cm^{-2} is observed for $PbS/BiVO_4$ photoanode working both in the dark and under illumination and it is ascribed to a double-layer capacitance. The Nyquist plots in the dark and under illumination (**Figure 4**b) showed a clear decrease of the charge transfer resistance under illumination. Additionally, a sharp increase in the imaginary part of the

Nyquist plot, i.e. the capacitance, under illumination reflects the accumulation of charge in the heterostructure.

In order to evaluate the PbS/$BiVO_4$ electrode as energy harvester beyond photoanode for solar water splitting, the photocharge and discharge of the electrode were studied in three-electrode configuration, for a more fundamental understanding. [48] The stability of the open circuit potential (OCP) reached after full photocharging of the device, and further charge delivery in dark conditions were also tested. To ensure the full charging of the photocapacitive device, the PbO_x/$BiVO_4$ electrode was wired to the Pt counter electrode and illuminated at 100 mW cm^{-2} for 30 s, under short-circuit conditions. Then, the cell was again connected in three-electrode configuration, and the OCP was measured for 1 hour in dark conditions, as showed in **Figure 4c** maintaining a value of around 1.1 V vs RHE, ensuring the high stability of the photocharged electrode for more than 60 minutes. The OCP value should correlate to the difference between the electron quasi-Fermi level and the hole quasi-Fermi level at the PbO_x interfacial layer electrode, and a value of around 1.45 V vs RHE should be expected. The lower OCP value obtained in this system confirms the presence of sulphide/sulphate lead species together with the formed PbO. The charge delivery capability in dark conditions was further evaluated, through galvanostatic discharge measurements at different discharge currents, as depicted in **Figure 4d**. The nonlinear discharge curves, particularly at lower discharge currents, evidence the Faradaic processes in the energy storage mechanism at the PbS/$BiVO_4$ photoanode. The output energy and power density calculated for the discharge current of 0.02 mA cm^{-2} are 0.35 μWh cm^{-2} and 12.6 μW cm^{-2}, respectively, according to the equations:[49] $E\ (Whcm^{-2}) = \int_0^{t_d} V \cdot j \cdot dt/3600$ and $P\ (Wcm^{-2}) = E/t_d$, where j is the current density (A·cm^{-2}) and t_d is the discharge time (s). The efficiency of solar energy conversion to energy storage can be considered as the sum of the energy stored in the H_2 molecule plus the charge stored in the PbS/$BiVO_4$ photoanode. Here, a full photoelectrochemical cell is not assembled and we focus on the added energy accumulated as charge in the PbS/$BiVO_4$. The energy conversion-output electricity is estimated as 0.042 % according to the expression:[50] $\eta = (\int_0^{t_d} V \cdot j \cdot dt/P_l t_l) \cdot 100$, where t_l the time of irradiation (30 s) with illumination power P_l, here j and P_l are normalized by area (cm^2). This value is of the same order compared to that recently obtained in a redox flow battery coupled to a Z-scheme water splitting cell (0.01%).[9b] Few μW/cm^2 are estimated to be enough to power

microdevices. As an example, 10 μW is generally enough for a sensor to measure and transmit temperature readings every 5 seconds.[51] Consequently, the power output provided by the PbS/$BiVO_4$ system in the dark could be sufficient to transmit a signal in these conditions.

Conclusions

In summary, PbS nanocubes have been produced by a simple solvothermal synthesis, with good morphological and size control. Combined with $BiVO_4$, which is an extensively material studied as photoanode for solar water splitting, we have demonstrated that an added energy storage is possible in the system as a photocapacitance. Structural, optical and electrochemical study of $BiVO_4$ and PbS materials validate the injection of photogenerated holes at the $BiVO_4$ into the PbS nanocubes leading to its transformation to PbO_x, according to the estimated energy diagram. PbO_x/$BiVO_4$ works as a photocapacitor with an efficiency of 0.042 % and providing a power of 12.6 μW cm^{-2}.

Acknowledgements

We acknowledge financial support from the Ministerio de Ciencia, Innovación y Universidades of Spain through the project ENE2017-85087-C3-1-R and Ramon y Cajal Fellowship (Grant No. RYC-2018-025222-I). Universitat Jaume I is also acknowledged for funding (project UJI – B2018-71). Université de Tunis El-Manar also acknowledge the tunisian Ministry of Higher Education and Scientific Research (MHESR) for the financial support of this work

References

[1] J. H. Kim, D. Hansora, P. Sharma, J. W. Jang, J. S. Lee, *Chemical Society reviews* **2019**, *48*, 1908-1971.

[2] aY. Y. Birdja, E. Pérez-Gallent, M. C. Figueiredo, A. J. Göttle, F. Calle-Vallejo, M. T. M. Koper, *Nature Energy* **2019**, *4*, 732-745; bK. Sayama, *ACS Energy Letters* **2018**, *3*, 1093-1101; cP. Lanzafame, S. Abate, C. Ampelli, C. Genovese, R. Passalacqua, G. Centi, S. Perathoner, *ChemSusChem* **2017**, *10*, 4409-4419.

[3] T. Uekert, M. F. Kuehnel, D. W. Wakerley, E. Reisner, *Energy & Environmental Science* **2018**, *11*, 2853-2857.

[4] S. J. Varma, K. Sambath Kumar, S. Seal, S. Rajaraman, J. Thomas, *Advanced Science* **2018**, *5*, 1800340.

[5] O. Groeger, H. A. Gasteiger, J.-P. Suchsland, *Journal of the Electrochemical Society* **2016**, *163*, X3-X3.

[6] E. O'Shaughnessy, D. Cutler, K. Ardani, R. Margolis, *Applied Energy* **2018**, *213*, 11-21.

[7] J. Liu, Z. Bao, Y. Cui, E. J. Dufek, J. B. Goodenough, P. Khalifah, Q. Li, B. Y. Liaw, P. Liu, A. Manthiram, Y. S. Meng, V. R. Subramanian, M. F. Toney, V. V. Viswanathan, M. S. Whittingham, J. Xiao, W. Xu, J. Yang, X.-Q. Yang, J.-G. Zhang, *Nature Energy* **2019**, *4*, 180-186.

[8] R. Schmuch, R. Wagner, G. Hörpel, T. Placke, M. Winter, *Nature Energy* **2018**, *3*, 267-278.

[9] aF. Urbain, S. Murcia-López, N. Nembhard, J. Vázquez-Galván, C. Flox, V. Smirnov, K. Welter, T. Andreu, F. Finger, J. R. Morante, *Journal of Physics D: Applied Physics* **2018**, *52*, 044001; bZ. Li, W. Wang, S. Liao, M. Liu, Y. Qi, C. Ding, C. Li, *Energy & Environmental Science* **2019**, *12*, 631-639; cK. Wedege, D. Bae, W. A. Smith, A. Mendes, A. Bentien, *The Journal of Physical Chemistry C* **2018**, *122*, 25729-25740; dK. Wedege, D. Bae, E. Dražević A. Mendes, P. C. K. Vesborg, A. Bentien, *RSC Advances* **2018**, *8*, 6331-6340.

[10] F. Sahli, J. Werner, B. A. Kamino, M. Bräuninger, R. Monnard, B. Paviet-Salomon, L. Barraud, L. Ding, J. J. Diaz Leon, D. Sacchetto, G. Cattaneo, M. Despeisse, M. Boccard, S. Nicolay, Q. Jeangros, B. Niesen, C. Ballif, *Nature Materials* **2018**, *17*, 820-826.

[11] K. Lin, J. Xing, L. N. Quan, F. P. G. de Arquer, X. Gong, J. Lu, L. Xie, W. Zhao, D. Zhang, C. Yan, W. Li, X. Liu, Y. Lu, J. Kirman, E. H. Sargent, Q. Xiong, Z. Wei, *Nature* **2018**, *562*, 245-248.

[12] aS. Ahmad, C. George, D. J. Beesley, J. J. Baumberg, M. De Volder, *Nano Letters* **2018**, *18*, 1856-1862; bN. Vicente, G. Garcia-Belmonte, *The Journal of Physical Chemistry Letters* **2017**, *8*, 1371-1374.

[13] aZ. Sun, Z. Liu, J. Li, G.-a. Tai, S.-P. Lau, F. Yan, *Advanced Materials* **2012**, *24*, 5878-5883; bR. Saran, R. J. Curry, *Nature Photonics* **2016**, *10*, 81-92.

[14] aG.-H. Kim, F. P. García de Arquer, Y. J. Yoon, X. Lan, M. Liu, O. Voznyy, Z. Yang, F. Fan, A. H. Ip, P. Kanjanaboos, S. Hoogland, J. Y. Kim, E. H. Sargent, *Nano Letters* **2015**, *15*, 7691-7696; bC.-H. M. Chuang, P. R. Brown, V. Bulović

M. G. Bawendi, *Nature Materials* **2014**, *13*, 796-801; cG. H. Carey, A. L. Abdelhady, Z. Ning, S. M. Thon, O. M. Bakr, E. H. Sargent, *Chemical Reviews* **2015**, *115*, 12732-12763; dZ. Liu, J. Yuan, S. A. Hawks, G. Shi, S.-T. Lee, W. Ma, *Solar RRL* **2017**, *1*, 1600021.

[15] aM. Navaneethan, K. D. Nisha, S. Ponnusamy, C. Muthamizhchelvan, *Reviews on Advanced Materials Science* **2009**, *21*, 217-224; bX. Gong, Z. Yang, G. Walters, R. Comin, Z. Ning, E. Beauregard, V. Adinolfi, O. Voznyy, E. H. Sargent, *Nature Photonics* **2016**, *10*, 253-257.

[16] P. T. Guerreiro, S. Ten, N. F. Borrelli, J. Butty, G. E. Jabbour, N. Peyghambarian, *Applied Physics Letters* **1997**, *71*, 1595-1597.

[17] J. D. Patel, F. Mighri, S. E. Abdellah Ajji, *Materials Sciences and Applications* **2012**, *3*, 125-130.

[18] A. Sasaki, Y. Tsukasaki, A. Komatsuzaki, T. Sakata, H. Yasuda, T. Jin, *Nanoscale* **2015**, *7*, 5115-5119.

[19] aV. S. R. R. Pullabhotla, M. Ngcobo, *Materials Letters* **2017**, *198*, 156-159; bD. C. Onwudiwe, *Heliyon* **2019**, *5*, e01413.

[20] Z. Zhang, S. H. Lee, J. J. Vittal, W. S. Chin, *The Journal of Physical Chemistry B* **2006**, *110*, 6649-6654.

[21] D. Yu, D. Wang, Z. Meng, J. Lu, Y. Qian, *Journal of Materials Chemistry* **2002**, *12*, 403-405.

[22] S.-M. Lee, Y.-w. Jun, S.-N. Cho, J. Cheon, *Journal of the American Chemical Society* **2002**, *124*, 11244-11245.

[23] aS. Xiong, B. Xi, D. Xu, C. Wang, X. Feng, H. Zhou, Y. Qian, *The Journal of Physical Chemistry C* **2007**, *111*, 16761-16767; bT. Mandal, G. Piburn, V. Stavila, I. Rusakova, T. Ould-Ely, A. C. Colson, K. H. Whitmire, *Chemistry of Materials* **2011**, *23*, 4158-4169.

[24] aK. Singh, A. A. McLachlan, D. G. Marangoni, *Colloids and Surfaces A: Physicochemical and Engineering Aspects* **2009**, *345*, 82-87; bN. B. Pendyala, K. S. R. K. Rao, *Materials Chemistry and Physics* **2009**, *113*, 456-461; cG. Li, C. Li, H. Tang, K. Cao, J. Chen, *Materials Research Bulletin* **2011**, *46*, 1072-1079.

[25] J. Muro-Cruces, A. G. Roca, A. López-Ortega, E. Fantechi, D. del-Pozo-Bueno, S. Estradé, F. Peiró, B. Sepúlveda, F. Pineider, C. Sangregorio, J. Nogues, *ACS Nano* **2019**, *13*, 7716-7728.

[26] aS. Acharya, D. D. Sarma, Y. Golan, S. Sengupta, K. Ariga, *Journal of the American Chemical Society* **2009**, *131*, 11282-11283; bC. Schliehe, B. H. Juarez, M. Pelletier, S. Jander, D. Greshnykh, M. Nagel, A. Meyer, S. Foerster, A. Kornowski, C. Klinke, H. Weller, *Science* **2010**, *329*, 550; cM. S. Bakshi, P. Thakur, S. Sachar, G. Kaur, T. S. Banipal, F. Possmayer, N. O. Petersen, *The Journal of Physical Chemistry C* **2007**, *111*, 18087-18098.

[27] C. Zhang, Z. Kang, E. Shen, E. Wang, L. Gao, F. Luo, C. Tian, C. Wang, Y. Lan, J. Li, X. Cao, *The Journal of Physical Chemistry B* **2006**, *110*, 184-189.

[28] S. Safshekan, I. Herraiz-Cardona, D. Cardenas-Morcoso, R. Ojani, M. Haro, S. Gimenez, *ACS Energy Letters* **2017**, *2*, 469-475.

[29] Y. Ma, F. Le Formal, A. Kafizas, S. R. Pendlebury, J. R. Durrant, *Journal of Materials Chemistry A* **2015**, *3*, 20649-20657.

[30] E. Burstein, S. Perkowitz, M. H. Brodsk, *Journal de Physique Colloques* **1968**, *29*, 78-83.

[31] D. Zhou, L.-X. Pang, J. Guo, Z.-M. Qi, T. Shao, Q.-P. Wang, H.-D. Xie, X. Yao, C. A. Randall, *Inorganic Chemistry* **2014**, *53*, 1048-1055.

[32] A. H. Khan, R. Brescia, A. Polovitsyn, I. Angeloni, B. Martín-García, I. Moreels, *Chemistry of Materials* **2017**, *29*, 2883-2889.

[33] P. W. Voorhees, *Journal of Statistical Physics* **1985**, *38*, 231-252.

[34] Y. Li, Y. Hu, S. Peng, G. Lu, S. Li, *The Journal of Physical Chemistry C* **2009**, *113*, 9352-9358.

[35] M. Bashouti, E. Lifshitz, *Inorganic Chemistry* **2008**, *47*, 678-682.

[36] L. Dong, Y. Chu, Y. Zhuo, W. Zhang, *Nanotechnology* **2009**, *20*, 125301.

[37] A. Hagarman, T. Measey, R. S. Doddasomayajula, I. Dragomir, F. Eker, K. Griebenow, R. Schweitzer-Stenner, *The Journal of Physical Chemistry B* **2006**, *110*, 6979-6986.

[38] L. Cademartiri, E. Montanari, G. Calestani, A. Migliori, A. Guagliardi, G. A. Ozin, *Journal of the American Chemical Society* **2006**, *128*, 10337-10346.

[39] A. Aghassi, M. Jafarian, I. Danaee, F. Gobal, M. G. Mahjani, *Journal of Electroanalytical Chemistry* **2011**, *661*, 265-269.

[40] C.-Y. Lin, C.-Y. Teng, T.-L. Li, Y.-L. Lee, H. Teng, *Journal of Materials Chemistry A* **2013**, *1*, 1155-1162.

[41] O. A. Carrasco-Jaim, O. Ceballos-Sanchez, L. M. Torres-Martínez, E. Moctezuma, C. Gómez-Solís, *Journal of Photochemistry and Photobiology A: Chemistry* **2017**, *347*, 98-104.

[42] L.-D. Zhao, J. He, S. Hao, C.-I. Wu, T. P. Hogan, C. Wolverton, V. P. Dravid, M. G. Kanatzidis, *Journal of the American Chemical Society* **2012**, *134*, 16327-16336.

[43] aM. Huang, J. Bian, W. Xiong, C. Huang, R. Zhang, *Journal of Materials Chemistry A* **2018**, *6*, 3602-3609; bE. S. Kim, H. J. Kang, G. Magesh, J. Y. Kim, J.-W. Jang, J. S. Lee, *ACS Applied Materials & Interfaces* **2014**, *6*, 17762-17769.

[44] T. Xu, R. Zhu, G. Zhu, J. Zhu, X. Liang, Y. Zhu, H. He, *Applied Catalysis B: Environmental* **2017**, *212*, 50-58.

[45] Y. Batonneau, C. Brémard, J. Laureyns, J. C. Merlin, *Journal of Raman Spectroscopy* **2000**, *31*, 1113-1119.

[46] M. Haro, C. Solis, V. M. Blas-Ferrando, O. Margeat, S. B. Dhkil, C. Videlot-Ackermann, J. Ackermann, F. Di Fonzo, A. Guerrero, S. Gimenez, *ChemSusChem* **2016**, *9*, 3062-3066.

[47] P. Delahay, M. Pourbaix, P. V. Rysselberghe, *Journal of The Electrochemical Society* **1951**, *98*, 57.

[48] W. G. Pell, B. E. Conway, *Journal of Power Sources* **2004**, *136*, 334-345.

[49] F. Zhang, T. Zhang, X. Yang, L. Zhang, K. Leng, Y. Huang, Y. Chen, *Energy & Environmental Science* **2013**, *6*, 1623-1632.

[50] D. Lau, N. Song, C. Hall, Y. Jiang, S. Lim, I. Perez-Wurfl, Z. Ouyang, A. Lennon, *Materials Today Energy* **2019**, *13*, 22-44.

[51] R. J. M. Vullers, R. v. Schaijk, H. J. Visser, J. Penders, C. V. Hoof, *IEEE Solid-State Circuits Magazine* **2010**, *2*, 29-38.

Table of contents:

PbS nanocubes have been synthesised by a simple solvothermal method with good morphological and size control and have been deposited on spin-coated $BiVO_4$ photoanodes to form a p-n junction showing synergistic photocapacitive properties. $PbO_x/BiVO_4$ system works as a photocapacitor with a solar-to-current efficiency of 0.042 %, providing a power density of 12.6 µW cm^{-2}.

Keyword: $PbS/BiVO_4$ Photocapacitor

Amira Lemsi,[1] Drialys Cárdenas-Morcoso,[2] Marta Haro,[3] Carlos Gil-Barrachina,[2] Clara Aranda,[2] Hager Maghraoui-Meherzi,[1] Miguel García-Tecedor,[2,*] Sixto Giménez,[2,*] Beatriz Julián-López[2,*]

Title: PbS nanocubes for solar energy storage